# Topology of slightly polydisperse real foams

C. Monnereau,* B. Prunet-Foch, and M. Vignes-Adler†
*LPMDI, FRE 2395 du CNRS, Bâtiment Lavoisier, Université de Marne-la-Vallée, F-77454 Marne-la-Vallée Cedex 2, France*
(Received 16 August 1999; revised manuscript received 27 February 2001; published 21 May 2001)

The topology of slightly polydisperse, (meta-)stable, real foams was investigated by means of optical tomography associated with a numerical reconstruction procedure. The values of the mean numbers of faces per bubble and edges per face were very close to Matzke's data (1946). The real foams were essentially disordered and possessed a noncentered symmetry, and ideal structures also could not be observed. The disorder was quantified by the second moment of the edge per face and face per bubble distributions, and also by a statistical correlation coefficient between the numbers of edges of adjacent faces. It was found that the edge distributions of the internal bubbles, and not of the external ones, were significantly anticorrelated even during foam aging, which provided a measure of the disorder in the foam. No obvious relationship could be deduced between the isoperimetric quotient and the face combination in an individual bubble. Eventually, it was shown that the physical boundaries of the foam sample had no influence on the foam topology beyond a single bubble layer.

DOI: 10.1103/PhysRevE.63.061402 PACS number(s): 82.70.Rr

## I. INTRODUCTION

In recent years many efforts have been devoted to the numerical simulation of three-dimensional (3D) dry foams, the ultimate aim has been to perform numerical experiments [1,2,3]. However, any numerical simulation requires some basic and quantified knowledge of the foam structure to be experimentally validated.

In a dry 3D liquid foam, bubbles are polyhedral-like and their structures are therefore complex. Moreover, a foam is never in stable thermodynamic equilibrium, and due to its very high energy and its large surface it evolves toward either a metastable state or its destruction. Even a long standing foam suffers some rearrangement as time elapses because of the coarsening phenomenon.

The foam local structure is such that the liquid films organize themselves to minimize their surface energy for a given gas volume according to the Laplace and Plateau laws. Provided the film tension is everywhere constant in the foam,[1] (i) each liquid film has a constant mean curvature, (ii) the edges (Plateau borders) are formed by three liquid films with mutual angles equal to 120°, and (iii) the vertices are formed by four edges with mutual angles equal to the tetrahedral angle, $\cos^{-1}(-\frac{1}{3})$. The film network reorganizes as time elapses because of film ruptures (coalescence) or gas diffusion from a smaller bubble towards a bigger neighbor due to the difference in Laplace's pressure (coarsening). Morphological recombinations are therefore induced and topological changes (T1) that involve bubble neighbor switching, or topological transformations (T2) when a bubble disappears can be observed. Eventually, the global structure of the foam is space filling [4].

In this work, we are interested in the structural and topological properties of real dry foams. Their polyhedral-like bubbles have various numbers of faces as well as various numbers of edges. Quantification of the foam structure requires basic topological measurements, e.g., the number of edges for a given face $n$ and the number of faces for a given bubble $f$ and their combinations, respectively, in a bubble and in the foam. From these data the statistical characteristics of the foam such as the average number of faces per bubble $\langle f \rangle$, the average number of edges per face $\langle n \rangle$, and the probability for a bubble to have $f$ faces, denoted by $p_b(f)$, and for a face to have $n$ edges, denoted by $p_f(n)$, are deduced. Moreover, polyhedral real foams have usually no periodic structure since they are essentially disordered. Hence, disorder is an additional foam property to quantify. By enforcing the angles values, the Plateau laws, which are somewhat antagonist with disorder, impose a severe constraint on the bubble polyhedral structure, which prevent the foam from being a disorganized system; moreover, the global stucture should ''divide space with minimum partitional area'' as stated by Kelvin [5]. In this context, we have measured the isoperimetric quotient $I_Q$ of each polyhedral bubble, which compares the bubble area to the one of a sphere with the same volume, and we have explored whether a relationship between the topology and the isoperimetric quotient of the bubbles could be obtained. For a comprehensive analysis of the foam characterization, one must remember that they are finite systems that are limited by physical boundaries, namely, the container walls or the foam-free surface depending on the experimental conditions. This implies singularities in the system and breaks the geometrical symmetries observed in the bulk foam since the Plateau laws are no longer valid at the artifactual vertices located on the solid walls. Two bubble populations have therefore to be considered, namely, the internal bubbles that belong to the bulk foam and the external bubbles that are adjacent to the boundaries. This distinction is particularly relevant when a flowing foam is

*Present address: Department of Physics, Trinity College, University of Dublin, Dublin 2, Ireland. Email address: Michele.Adler@univ-mlv.fr

†Author to whom correspondence should be addressed.

[1]Throughout the paper, we have assumed that the film tension is constant everywhere and that the foam free energy can be reduced to the film surface free energy.

 

investigated, e.g., shear stress at the wall may be transmitted to the internal bubbles through the external ones located at the solid boundary.

Most studies on foam topology deal with the theoretical solution to the Kelvin problem and some ideal structures, namely, the Kelvin tetrakaidecahedron [5], the Williams cell [6], and the Weaire and Phelan cluster [7] were proposed. As far as we know, these ''perfect'' stuctures could only be observed under very special boundary conditions, but not in real bulk foam [8].

Actually, there are only a few experimental investigations on real foam structure because the internal structure of a 3D foam is difficult to observe. The first experiment on the structure of a 3D foam was done by Matzke [9]. Matzke used a binocular dissecting microscope to examine each single bubble of a 3D monodisperse foam. The foam was generated a bubble at a time using a graduated syringe and putting it after its creation into a beaker. The bubbles were then drawn by means of a camera lucida. Matzke could therefore obtain the description of the topology of a monodisperse foam at a given time, assuming that neither coarsening nor topological transformation occurred during the time the photographs were taken. He found that the average number of faces per bubble $\langle f \rangle = 11.00$ for 400 bubbles belonging to the first three layers and $\langle f \rangle = 13.7$ for the 600 internal bubbles, which he defined as the bubbles separated by at least three layers of bubbles from the surface. He also listed the combinations of both populations. Schwarz described the topological transformations that may occur in 3D collapsing foams [10] and photographed face swapping between two adjacent bubbles.

Thanks to the computer age, we can reproduce and extend Matzke's original experiments. We have simultaneously measured the structure and the metric properties of 3D foams [11–13] by an optical tomographic method in association with a numerical reconstruction. From these measurements, we can access simultaneously the metrics and topology of the foam when it is young and also when it is aged and collapsing.

## II. EXPERIMENT

### A. Materials and methods

The cell consists of a cylindrical container (5 cm diameter and 10 cm height) covered by a glass lid, whose lower part is a sintered glass plate (Fig. 1). Its bottom is connected to a liquid reservoir by a flexible Teflon tube in order to control the capillary pressure $P_\gamma \approx \rho g \Delta h$ in the foam by changing the height level $\Delta h$ between the container and the reservoir [14]. $\Delta h$ is measured by a cathetometer. Both container and reservoir are fixed to the same motorized table (z) in order to keep $\Delta h$ constant during scanning. In the whole experiment, $\Delta h$ is fixed at 60 mm, i.e., $P_\gamma \approx 595$ Pa. Therefore, the Plateau border curvatures are kept nearly constant along the foam column and during the dynamic experiment, and the film thicknesses can also be considered as being constant along the foam column and during the dynamic experiment.

In order to prevent contamination by antifoaming materials, great care was taken in cleaning the cell. After degreasing with acetone (Normapur) and alcohol, the glassware was washed with fresh sulfochromic acid, the Teflon tube with boiling aquaregia, followed by profusely rinsing with pure water. The cell was filled with two different soapy solutions: an aqueous solution of sodium dodecyl sulfate (0.1% wt) and dodecanol (0.003% wt) (solution *A*), and another aqueous solution of commercial hand liquid soap (0.3% wt) and glycerol (0.2% wt) (solution *B*). Slightly polydisperse foams with a mean diameter bubble size of $5 \pm 2$ mm were then generated in the cylindrical container by blowing filtered *U* nitrogen through a pro-Pasteur pipette directly in the solution at a flow rate of 55 $mm^3 s^{-1}$. The films of both soapy solutions in these proportions immediately evolve into common black films. They are extremely stable in time [13], moreover their surfaces are rigid according to the classification given by Mysels, Shinoda, and Frankel [15]. This means that the surface-active materials form a layer so compact at the interface that no interfacial convection occurs; gravity drainage in the Plateau borders is drastically reduced and the gas transfer between two bubbles is solely diffusional. This was numerically confirmed by coarsening calculations with SURFACE EVOLVER[2] [16].

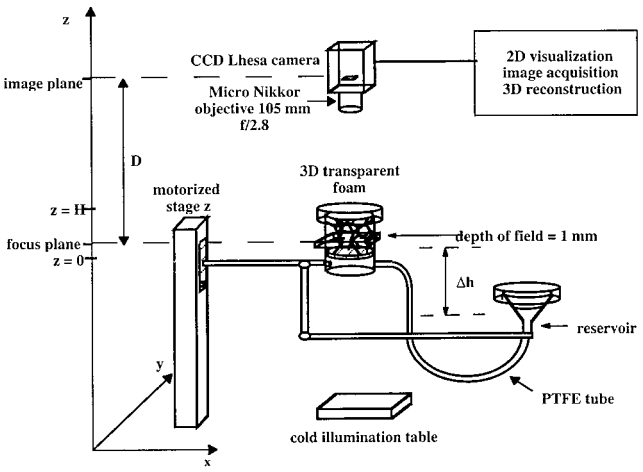


FIG. 1. Experimental setup.

### B. Optical tomography and foam reconstruction

The cell was lit with a cold and polarized illumination plate (Fig. 1). Optical tomography consisted in scanning the foam by means of a Lhesa charge-coupled device camera equipped with a very thin depth-of-field (1 mm thick) Micro-Nikkor 105 mm f/2.8 objective and connected to a graphic digitization card. The camera was focused on the center of the upper surface of a foam sample to visualize only the bubbles without any contact with the cell walls. During scanning, the optical system was kept fixed while the foam cell was displaced in the focus plane by steps equal to $\Delta z = 1$ mm. Images of the slices were digitized and stored in a microcomputer. A whole scanning session took 45 s for 30

[2]SURFACE EVOLVER is a minimization software developed by Brakke [17].

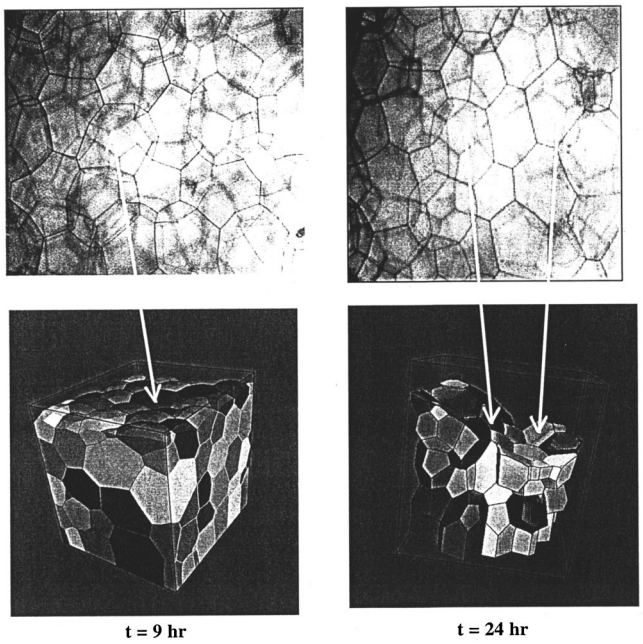


FIG. 2. Upper row: Images of slices of foam 2 located at a same z in the central parallelepipedic core ($2.2\times1.6\,cm^2$) at $t=9$ h and $t=24$ h. The coordinate system is given in Fig. 1. The optical field is located at the center of the cylindrical foam column whose internal diameter is $\varnothing=5$ cm. Only the sharp vertices belong to the plane $z_0$; the fuzzy vertices belong to neighbor slices. Lower row: Reconstructed foam 2 at $t=1$ h and $t=24$ h. The white arrows relate corresponding bubbles.

slices. Since nitrogen has a low solubility in water, foam coarsening was negligible during the time of scanning.

A picture of a foam slice in the central parallelepiped core ($2.2\times1.6\,cm^2$) of the foam column ($\varnothing=5$ cm) is given in Fig. 2. The liquid films are transparent since they are common black films and only the Plateau border (edge) network appears in the images. The principle of foam reconstruction is to determine the locations of all the foam vertices from a series of such images of foam slices using a specific image software (MOUSSE), and to numerically reconstruct the minimal surfaces connecting the vertices in the same polyhedral arrangement as the real foam using SURFACE EVOLVER[3] [18]. The physical assumption underlying the reconstruction procedure of very dry foams is that capillarity is solely acting on the foam structure. The structure is minimized under the constraints that the bubble volumes are constant; the positions of the outer vertices on the sample lateral boundaries and on the foam-free surface are fixed (when only entire bubbles are reconstructed); the positions of the vertices in contact with the porous plate and of the intersections with the digitization window limit (when also the boundary bubbles are reconstructed) are free to move in their plane; all the other vertices in the bulk foam are free to move. The equilibrium structure of the foam is such that the surface energy is minimum for the given structure and gas phase volume. The so-called reconstructed foam is the one whose total surface area of the films is minimized, Laplace's law and Plateau's law being satisfied (Fig. 2). The whole reconstruction procedure has been described in greater detail in [18]. On the reconstructed foam, the topological and metric properties can be measured and then analyzed.

[3]MOUSSE is a foam analyzer software from Noesis Inc., SURFACE EVOLVER compatible.

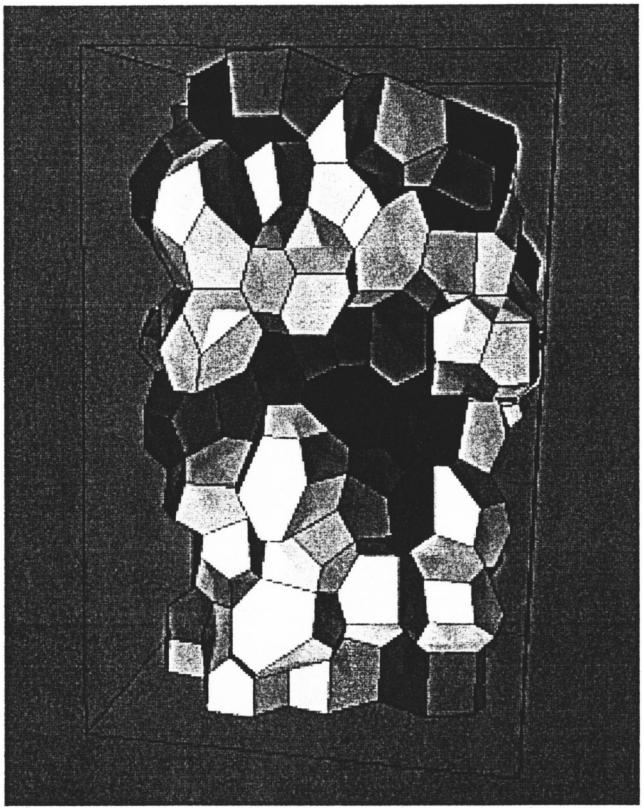

FIG. 3. Entire bubbles of reconstructed foam 1 showing the volume polydispersity; there are five classes of bubble volumes ranging from 38 to 61 $mm^3$.

## III. RESULTS

We have studied and reconstructed two foams made from solution *A* denoted below as foam 1 and foam 2, and a third one made from solution *B* called foam 3. Only the dynamics of foam 2 was followed during 30 h. Let us note that bubbles are called *entire* when they are not artifactually cut by the optical field (Fig. 2); bubbles are called *boundary bubbles* when only a percentage of their faces is known since they are cut by the optical field. Foam 1 consisted of 8 bubble layers among which 82 entire bubbles were analyzed (Fig. 3). Foam 2 consisted of 144 bubbles organized in 5 layers of bubbles among which 48 bubbles were entire (Fig. 2 left column). Foam 3 consisted of 121 bubbles organized in 5 layers with 41 entire bubbles.

One should distinguish two types of bubbles, (i) the *external bubbles* that belong to the upper layer or to the bottom one in contact with the porous plate and (ii) *the internal bubbles* that belong to the other layers. The internal bubbles have all their neighboring ones in the real foam.

We have gathered all the data of the three independent

TABLE I. Topological characteristics of the bubbles in the young foams 1, 2, and 3. $N$ (bubble number), $F$ (number of discernible faces), $V$ (bubble average volume), $\Delta V$ (standard deviation of bubble volume distribution), $\langle f \rangle$ (mean face/bubble), $\langle n \rangle$ (mean edge/face), $\langle f \rangle_{\text{th}}$ [theoretical mean face/bubble as calculated by Eq. (1)], $\mu_{2f}$ (second moment of face distribution), $\mu_{2n}$ (second moment of edge distribution), $R$ (edge correlation coefficient. The common faces to two adjacent bubbles were counted twice by Matzke).

| | $N$ | $F$ | $\Delta V/V$ | $\langle f \rangle$ | $\langle f \rangle_{\text{th}}$ | $\langle n \rangle$ | $\mu_{2\,f}$ | $\mu_{2n}$ | $R$ |
|---|---|---|---|---|---|---|---|---|---|
| | | | | External upper layer | | | | | |
| Foam 1 | 16 | 145 | 0.22 | 11.19 | 11.76 | 4.98 | 5.03 | 0.63 | −0.21 |
| Foam 2 | 9 | 94 | 0.4 | 11.56 | 12.37 | 5.03 | 3.36 | 0.54 | −0.17 |
| Foam 3 | 17 | 136 | 0.36 | 10.76 | 11.21 | 4.93 | 2.25 | 0.67 | −0.20 |
| Average | 42 | 375 | | 11.07 | 11.90 | 4.99 | 3.54 | 0.62 | |
| Matzke | 400 | | | 10.99 | 10.99 | 4.908 | 1.49 | 0.519 | |
| | | | | Internal bubbles | | | | | |
| Foam 1 | 57 | 556 | 0.1 | 13.75 | 13.48 | 5.11 | 0.85 | 0.41 | −0.27 |
| Foam 2 | 28 | 278 | 0.08 | 13.39 | 13.04 | 5.08 | 1.81 | 0.365 | −0.23 |
| Foam 3 | 24 | 221 | 0.29 | 13.54 | 12.24 | 5.02 | 3.66 | 0.42 | −0.22 |
| Average | 109 | 1055 | | 13.53 | 13.47 | 5.109 | 3.24 | 0.40 | |
| Matzke | 600 | 8221 | | 13.702 | 13.698 | 5.124 | 1.07 | 0.328 | |

reconstructed foams that have different topologies, foam 1, foam 2 before its collapse, and foam 3, that is, altogether 109 internal entire bubbles and 42 external entire bubbles of the upper layer to get average topological results. This is called the *average foam* below. Note that we have not considered the boundary bubbles in contact with the bottom plate because their topologies are biased since Plateau's laws do not apply to the vertices adhering to the sintered glass plate.

First of all we have checked that the present foams are slightly polydispersed at least as far as the young foams are concerned by calculating the standard variation of the bubble volume distribution in the foam. Results are reported in Table I, and in Fig. 3 polydispersity is emphasized by changing the gray color of the bubbles. The polydispersity is low with $\Delta V/V < 0.3$ for the internal bubbles and 0.4 for the upper external bubbles of the young foams, where $\Delta V$ is the volume standard deviation.

### A. Topological properties

The mean values of the edge number per face $\langle n \rangle$ and of the face number per bubble $\langle f \rangle$ are calculated for the various foams and the average foam (Table I). Results are in very good agreement with Matzke's measured values $\langle f \rangle_{\text{int}} = 13.70$ and $\langle f \rangle_{\text{ext}} = 10.99$ on his 1000-bubbled foam [9]. To evaluate the statistical bias we have determined that the fluctuations around $\langle f \rangle$ become lower than $\pm 0.05$ for 20 or more bubbles taken at random for calculation of $\langle f \rangle$.

The distribution of the number of faces per bubble, $p_b(f)$, and the distribution of the number of edges per face, $p_f(n)$ of the average foam are plotted in Figs. 4(a) and 4(b) for both the internal and external populations. For the face distribution, there is a peak at $f = 13$ for the internal bubbles and at $f = 11$ for the external upper bubbles. Ninety-nine percent of the internal bubbles have a number of faces ranging from 12 to 15. Only one internal bubble was a 19-hedron. Always more than 95% of the faces are either quadrilateral, pentagonal, or hexagonal, with a predominance of pentagonal faces; the edge distribution has a peak at $n = 5$ of about 0.6. The edge/face distributions, $p_{f_0}(n)$, for $f_0$-polyhedra are plotted in Figs. 5(a) and 5(b). The value of the peak at $n = 5$ increases to $p_{f_{0=12}}(5) = 0.8$ when it is only calculated for the dodecahedra. It means that the probability for dodecahedra to be pentagonal is rather high. However, the probability to get a dodecahedron is low (0.08).

### B. Combinations

The bubble structure in the foam is characterized by the combinations of the $n$-edged faces in $f$-faced bubbles. More

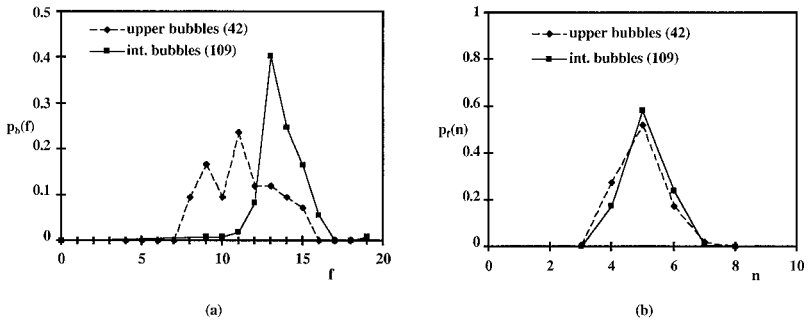


FIG. 4. Average foam: (a) Distribution $p_b(f)$ of the number $f$ of faces per bubble, (b) distribution $p_f(n)$ of the number $n$ of edges per face. The numbers in parentheses are the numbers of bubbles of the population under consideration.

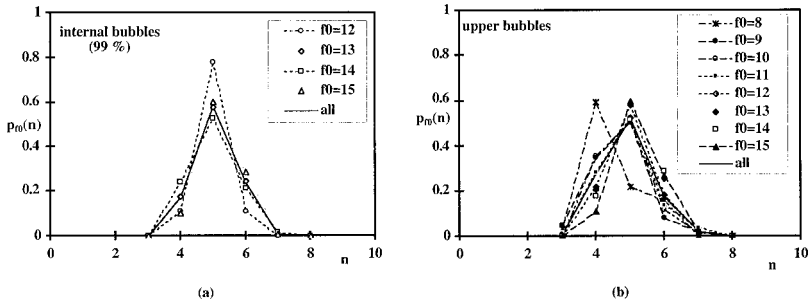


FIG. 5. Distribution $p_{f_0}(n)$ of the number of edges per face in the average foam, (a) internal bubbles, (b) upper external bubbles. The solid line denotes the mean distribution.

precisely, the numbers of 3- (if present), 4-, 5-, 6-, and 7-edged faces (if present), etc., were calculated and also their probability of occurrence. The list of the more frequent combinations is presented for each value of $f$ for the internal bubbles in Table II. The external bubbles[4] are shown in Table III. Matzke's combinations are also reported. There are five main combinations ($>5\%$) in the internal population with 13 and 14 faces and two in the external population, whereas Matzke found seven more frequent combinations that partly overlap ours. All the more frequent internal bubbles have more hexagonal than quadrilateral faces and it is the opposite for the external ones.

### C. Foam aging and collapse

Only foam 2 was reconstructed at 8 different times: $t=0$, 1, 3, 6, 9, 24, 27, and 30 h after its creation. Its topology did not change for the first 9 h, the structure remained the same and no topological transformation nor film rupture occurred. Note that this topological stability is due to the particular soapy solution that we have used. At $t=24$ h the foam was collapsed as observed by Brown, Thuman, and McBain who monitored the decay of a foam from the same soapy solution [19]. Films that were located on the top surface of the foam thinned, because of evaporation; the bubbles disproportionated due to the vicinity of the atmosphere (Fig. 2 right column). Film ruptures followed and generated other avalanche film ruptures in the neighborhood that are characteristic of the collapse of a dry foam with rigid films. The number of bubbles and faces are reported in Table IV. For the different times, $\langle f\rangle_{\mathrm{ext}}$ varies between 9.81 and 11.56 and $\langle f\rangle_{\mathrm{int}}$ between 13.39 and 13.67 even for the very destabilized foam at 30 h; the edge per face distributions $p_f^t(n)$ are reported for the internal bubbles in Fig. 6(a) and for the upper bubbles in Fig. 6(b). For the internal bubbles, the percentage of pentagonal faces increases whereas the percentage of quadrilateral faces decreases as time elapses, and it is the opposite for the upper ones; the distribution remains very stable during aging. Accordingly, internal combinations remained quite stable: no original combinations appeared that did not exist either in the average foam or in Matzke's one (Table III). The total number of internal bubbles drastically decreased when foam 2 collapsed, and we have reported the number of bubbles with a given combination and not the percentage of bubbles for the aged foams.

External upper bubbles were much more creative (Table V). One could identify 11 original combinations: 9-edged faces could be observed as a consequence of film ruptures and tetrahedral bubbles with 3-edged faces appeared as a consequence of disproportionation and T2 topological transformations. Furthermore, T1 face swappings between adjacent internal bubbles were observed, but they did not generate new combinations (Table IV). It is likely that neither Matzke nor we have identified all the possible combinations.

## IV. DISCUSSION

So far, we have mostly confirmed the results of Matzke who obtained them manually on an enormous number of bubbles. One can only be impressed by his extraordinary patience in collecting these data. Computer technology enables us to get more information since the bubble geometrical quantities can be measured in addition to the topological ones and the bubble arrangements in the foam can be determined, moreover, their time evolution can be followed.

### A. Topological properties

The average number of faces per internal bubble $\langle f\rangle$ and edges per face $\langle n\rangle$ obtained for our average foam satisfy the Coxeter theoretical relationship, which states that if the foam has an infinite number of internal bubbles, $\langle f\rangle_{\mathrm{th}}$ should be related to $\langle n\rangle$ as [20]

$$\langle f\rangle_{\mathrm{th}}=\frac{12}{6-\langle n\rangle}. \tag{1}$$

This relationship is well satisfied by the average foam (Table I). Besides, $\langle f\rangle$ is also in agreement with the predicted values of Aste, Boosé, and Rivier [21] who found that $\langle f\rangle$ should range between 13.29 and 13.5, the lower bound corresponding to configurations with a maximal orientational entropy and 13.5 to the Weaire-Phelan structure, which has the lowest known interfacial energy for equal-volume bubbles [21].

The structures that have the same face combinations as the ideal structures are denoted by bold face characters in Tables II and III; most frequently found is the (2 8 4) Williams cell, but without its centered symmetry. Neither Kelvin's bubble, the tetrakaidecahedron, which is a truncated octahedron (6 0 8), nor Weaire-Phelan's structure, which is a cluster of six 14-faced bubbles (0 12 2) and two 12-faced (0

[4]The complete list can be obtained upon request from Michele.Adler@univ-mlv.fr

TABLE II. Main face combinations and isoperimetric quotient of internal bubbles. The number within parenthesis is the $I_Q$ standard deviation. The combination of the Williams cell and the combinations present in Weaire-Phelan cell are in bold characters. Percentages are used for the average and the Matzke foams. The number of bubbles is used for aging foam 2. Other combinations exist; however, their probability is 1% or less.

| | | | | Aging foam 2 | | | |
|---|---|---|---|---|---|---|---|
| $f$ | Comb. 4 5 6 | Average (%) | Matzke (%) | $t=24$ h No. of bubbles | $t=27$ h No. of bubbles | $t=30$ h No. of bubbles | $I_Q$ |
| 13 | 3 6 4 | 17 | 6 | | | | 0.692 (0.0421) |
| 13 | 1 10 2 | 12 | 20 | 2 | 2 | 1 | 0.695 (0.0265) |
| **14** | **2 8 4**[a] | **9** | **11** | **2** | **2** | | **0.689 (0.0226)** |
| 14 | 1 10 3 | 7 | 12 | 1 | 1 | 1 | 0.699 (0.033) |
| 13 | 2 8 3 | 7 | 3 | 3 | 3 | 1 | 0.693 (0.0205) |
| 15 | 0 12 3 | 5 | 4 | | | | |
| 15 | 1 10 4 | 5 | 6 | 2 | 2 | | |
| 12 | 2 8 2 | 5 | 3 | 1 | 1 | | |
| **12** | **0 12 0**[b] | **4** | **8** | | | **1** | |
| **14** | **0 12 2**[b] | **2** | **7** | | | | |

[a]Williams cell.
[b]Weaire-Phelan cell.

12 0) bubbles, were found. The combination shown by the Kelvin bubble that has no pentagonal faces and more hexagonal than quadrilateral faces, seems far from the present results; the nearest that was obtained is a (6 0 2) combination among the upper layer bubbles of both foams 1 and 3 (Table III). In contrast, the two combinations that composed the Weaire-Phelan structure (0 12 2) and (0 12 0), with identically centered symmetry apart for the fact that the faces of

TABLE III. Main face combinations of external bubbles. The combination of the Williams cell and the combinations present in the Weaire-Phelan cell are in bold characters. Percentages are used for the average and the Matzke foams. The number of bubbles is used for the aging foam 2. Other combinations exist; however, their probability is 1% or less.

| | | | | Aging foam 2 | | |
|---|---|---|---|---|---|---|
| $f$ | Combinations 3-4 5 6-7 | % in Average | % in Matzke | $t=24$ h No. of bubbles | $t=27$ h No. of bubbles | $t=30$ h No. of bubbles |
| 9 | 4 4 1 | 9.5 | 2.8 | 2 | 1 | 3 |
| 11 | 4 5 1-1 | 7.1 | 5.5 | | | 1 |
| 10 | 3 6 1 | 4.8 | 7.3 | 2 | 1 | 2 |
| 11 | 3 6 2 | 4.8 | 16.8 | | | |
| 11 | 2 8 1 | 4.8 | 8.8 | | | 1 |
| 12 | 3 6 3 | 4.8 | 5.5 | | | |
| 10 | 4 4 2 | 4.8 | 11.8 | | 1 | 1 |
| 13 | 3 6 4 | 4.8 | 0.8 | 1 | | |
| 8 | 6 0 2 | 4.8 | 1.3 | | | |
| 15 | 3 7 4-1 | 4.8 | | | | |
| | | | Particular combinations | | | |
| **14** | **2 8 4**[a] | **2.4** | **0.8** | | | |
| **12** | **0 12 0**[b] | | **2.8** | | | **1** |
| **14** | **0 12 2**[b] | | **0.3** | | | |

[a]Williams cell.
[b]Weaire-Phelan cell.

TABLE IV. Topological characteristics of the foam bubbles of the aging foam 2.

| Foam 2 | $N$ | $P$ | $\Delta V/V$ | $\langle f \rangle$ | $\langle n \rangle$ | $\mu_{2\,f}$ | $\mu_{2n}$ | $R$ |
|---|---|---|---|---|---|---|---|---|
| | | | | External upper layer | | | | |
| $t \leqslant 9$ h | 9 | 94 | 0.4–0.6 | 11.56 | 5.03 | 3.36 | 0.54 | −0.17 |
| $t = 24$ h | 21 | 165 | 0.85 | 9.81 | 4.85 | 10.63 | 0.83 | 0.038 |
| $t = 27$ h | 17 | 135 | 0.75 | 9.88 | 4.86 | 11.16 | 0.95 | −0.018 |
| $t = 30$ h | 14 | 120 | 0.5 | 10.57 | 4.93 | 1.96 | 0.59 | −0.17 |
| | | | | Internal bubbles | | | | |
| $t \leqslant 9$ h | 28 | 278 | 0.08–0.15 | 13.39 | 5.08 | 1.81 | 0.365 | −0.23 |
| $t = 24$ h[a] | 12 | 140 | 0.17 | 13.67 | 5.11 | 0.89 | 0.34 | −0.22 |
| $t = 27$ h[a] | 12 | 140 | 0.20 | 13.67 | 5.11 | 0.89 | 0.34 | −0.22 |
| $t = 30$ h | 6 | 71 | 0.125 | 13.50 | 5.11 | 0.92 | 0.353 | (−0.31) |

[a]The topology of the internal bubbles, namely, the face and edge combinations did not change between $t = 24$ h and $t = 27$ h but the foam coarsened as $\Delta V/V$ increases.

the same kind do not have equal area, were found separately among the internal bubbles of *foam 1*; both have a probability of 4%. They were not connected and they did not form the Weaire-Phelan (WP) cluster.[5] It is remarkable that the WP structure has 89% of pentagons, which is much larger than the percentage ($\cong$60%) found in real foams; it is however consistent with our finding that 80% of the dodecahedral bubbles are pentagonal like the two dodecahedra in the WP cluster.

*A priori* the absence of any ideal structures is surprising since these structures are supposed to correspond to a minimum of surface energy. It was expected that ideal structures should be obtainable given the absence of gravity drainage, capillary suction, and the fact that coarsening is reduced due to the low solubility of the gas used in this study.

We propose three reasons to explain the absence of ideal structures.

(i) The numerical calculations are done on a set of monodisperse bubbles. In our experiments, the bubbles are monodisperse at their creation since they are generated at the tip of a single capillary by blowing nitrogen at a controlled flowrate. However, the bubbles are created neither simultaneously nor at the same location in the liquid column. A newly created foam is in a transient state, with very important coarsening effects for the more recently created bubbles. This results in polydispersity, albeit low (Table I).

(ii) The ideal structures are obtained by minimizing the total surface energy of the films and neglecting the gravitational energy. Most liquid in a foam is located in the Plateau borders and the corresponding gravitational energy should also be taken into account in the minimization process. However, the contribution of the Plateau border gravitational energy to the total foam energy was found to be insignificant even in a foam with thicker Plateau border [12], and this second point has probably less influence. Nevertheless, a young foam is considerably drained, its history and topology are definitely influenced by gravity. Since the scale of the bubble diameter, about 2–5 mm, is of the same order of magnitude as the capillary length $(\sigma/\rho g)^{1/2} \cong 2$ mm, one cannot neglect the rupture of symmetry induced by gravity on the pressure in the Plateau borders.

(iii) Minimization algorithms do not account for possible bubble coarsening. Specifically, in the WP cluster, all the bubbles have equal volume but not equal pressure and foam coarsening should result. It is likely that ideal structures might only be obtained in real bulk foam under microgravity conditions or with extremely small bubbles when the bubble gas is insoluble in the film liquid. These conditions are challenging.

Eventually, the predominance of pentagons can be easily explained. All the films of the present foams were common

TABLE V. New external bubble combinations observed in the ageing foam 2 that did not exist either in the young foams or in the Matzke foam.

| $f$ | Combinations 3-4 5 6-7-8-9 | No. of bubbles $t = 24$ h | No. of bubbles $t = 27$ h | No. of bubbles $t = 30$ h |
|---|---|---|---|---|
| 13 | 1-1 8 2-1 | 1 | | |
| 6 | 2-2 2 0 | 2 | | |
| 14 | 2-2 5 4-0-0-1 | 1 | 1 | |
| 5 | 2-3 0 0 | 1 | 1 | |
| 7 | 3-0 3 1 | 1 | | |
| 4 | 4-0 0 0 | 1 | 2 | |
| 15 | 3 6 7 | 1 | 1 | |
| 9 | 1-3 3 2 | | 1 | |
| 10 | 1-3 4 1-1 | | 1 | |
| 12 | 1-3 4 3-1 | | 1 | |
| 11 | 5 4 0-2 | | | 1 |

[5]The Weaire-Phelan structure has been once visualized in a shaving cream under a microscope [22]. None of the Matzke 1000 bubbles were of Kelvin type. Half a Kelvin cell could be observed on a cubic frame [23]. Pittet, Rivier, and Weaire could obtain Kelvin bubbles in unidimensional crystalline foams by generating monodisperse foams in cylindrical tubes with a single entire bubble filling the tube section [24]. The cylindrical symmetry shown by the Kelvin cell was therefore enforced by the frame in the former case and by the tube wall in the latter one.

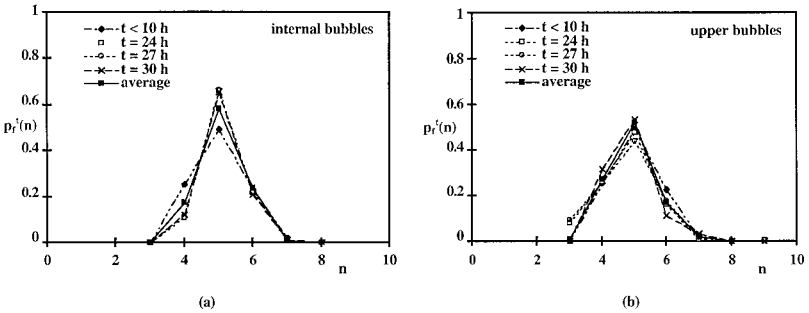


FIG. 6. Distribution $p_f(n)$ of the number of edges per face in the aging foam 2, (a) internal bubbles, (b) upper external bubbles. The solid line denotes the mean distribution.

black ones with film tensions equal to twice the solution surface tension acting at the vertices [25]. This enforces symmetry and explains the predominance of pentagons since the pentagonal angle 108° is very close to the regular tetrahedral angle $\arccos(-\frac{1}{3})$ ($\cong$109.5°). However, the pentagonal dodecahedra are not numerous in the present foams, which is not surprising since they cannot fill the whole space [26].

### B. Statistical analysis of the disorder

Real foams are disordered but they are not disorganized. This means that some quantification of the ''disorder'' in the structure should be obtained. The disorder of real foams can be partly characterized by the variances of the face and edge distributions defined as

$$\mu_{2,f}=\langle f^2\rangle-\langle f\rangle^2, \quad \mu_{2,n}=\langle n^2\rangle-\langle n\rangle^2 \tag{2}$$

by analogy with 2D foams [4]. The values are reported in Table I for the young foams and in Table IV for the aging foam 2. Furthermore, we have calculated Matzke's foam disorder from his data given in [9].

For the internal bubbles, the disorder calculated for the edge distribution $\mu_{2,n}$ is small, of order 0.4 and it is slightly higher, 0.6, for the external bubbles, which is close to Matzke's results. The disorder for the face distribution $\mu_{2,f}$ is larger and still of the same order of magnitude as Matzke. Both $\mu_{2,n}$ and $\mu_{2,f}$ remain constant during foam 2 aging.

For the external bubbles, both $\mu_{2,f}$ and $\mu_{2,n}$ increase significantly when the foam is ageing, because of T2 topological transformations and film ruptures (Fig. 2). However, their values decrease again when the foam is aged and small bubbles have disappeared.

To get more quantitative information on the foam disorder, we have explored whether some statistical correlation between the topological elements of the foam could be found. Let each face in the foam be numbered by the integer $j$; let $j_1$ and $j_2$ denote two adjacent faces in the foam, i.e., two faces with a common edge. The following correlation coefficient $R$ can, therefore, be calculated between the numbers of edges $n(j_1)$ and $n(j_2)$ of two adjacent faces with $j_1 \neq j_2$ for each population

$$R=\frac{\langle[n(j_1)-\langle n\rangle][n(j_2)-\langle n\rangle]\rangle}{\langle[n(j)-\langle n\rangle]^2\rangle}$$

$$=\frac{F_{\text{tot}}}{P}\frac{\sum_{j_1}\sum_{j_2<j_1}[n(j_1)-\langle n\rangle][n(j_2)-\langle n\rangle]}{\sum_{j}[n(j)-\langle n\rangle]^2}, \tag{3}$$

where $n(j)$ is the edge number of the $j$th face, $\langle n\rangle$ is the mean face number per bubble, $F_{\text{tot}}$ is the total number of different faces belonging to the considered bubble population, $P$ is the number of terms entering the double summation. We have ignored the biased faces, for example, the ones that intersect the boundary of the foam sample either at the porous plate or at the artifactual boundary of the optical field. For each foam, both populations were considered, namely, the internal bubbles and the upper layer bubbles. We have checked that $R$ becomes stable as soon as the number of pairs of faces $P$ that enters the summations is larger than 300. With $P=800$, the statistical error is $1/\sqrt{P}=0.05$.

The general trend is that the correlation coefficient $R$ is always negative whatever the value of $P$. The value of $R$ ranges between $-0.24$ and $-0.3$ for both bubble populations of the young foams 1, 2, and 3. This value is rather low, although significantly higher than the statistical error 0.05, even for the aged foam.[6] This means that the face distribution in the bulk foam is slightly anticorrelated, in other words, that the $2n$ neighbors of a face with a larger number of edges have statistically a smaller number of edges. As far as we know, this disorder quantification was never proposed. It provides a measure of the organization of the disorder in a slightly polydisperse foam.

It is interesting to note that $R_{\text{ext}}$ decreases to near 0 when measured on the upper external bubbles of the ageing foam 2 whereas the edge and face disorders are high (Fig. 7). It was observed that the collapse of the upper layer occurred like in an avalanche, which locally generated a very disordered foam with large values of $\mu_{2\,f}$ and $\mu_{2n}$, and bubbles with a very small number of faces appeared due to T2 transformations (Fig. 2). However, when the ''order'' in the foam is restored, the correlation coefficient $R$ recovers to its initial value ($=-0.17$). On the contrary, $R_{\text{int}}$ calculated for the internal bubbles remained constant during aging. Actually, in the present foam the structure of the internal population was only altered by face switching that globally occurred at constant face and edge numbers.

Unfortunately, the present sample was too small to obtain a reliable value of the correlation coefficient based on the face number of adjacent bubbles, which would give a 3D analog of the Aboav-Weaire law established for 2D foams [4]. This is left for future work.

[6]We have not reported the value of $R$ at $t=30$ h for internal bubbles because there are only 6 surviving bubbles.

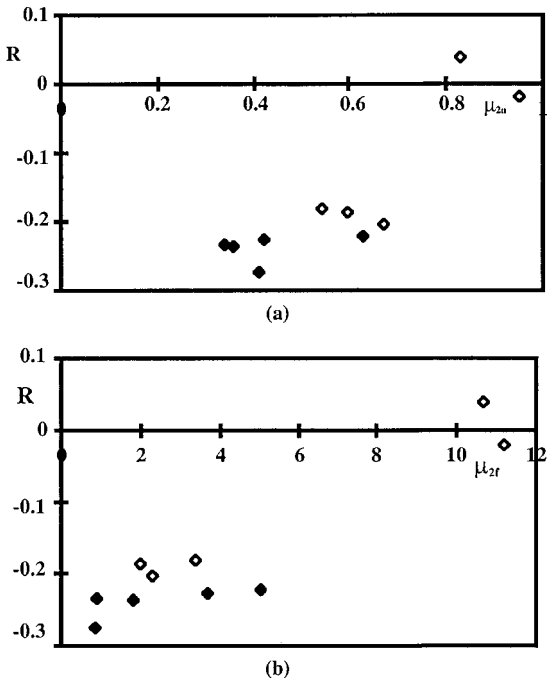


FIG. 7. Edge correlation coefficient $R$ versus (a) edge disorder, (b) face disorder. The full symbols denote the internal bubbles and the empty symbols the external upper bubbles.

### C. Topology and isoperimetric quotient

The isoperimetric quotient $I_Q$ was obtained from the volume and the area of the bubbles. $I_Q$ compares the area $S$ of a polyhedron to the area $S_0$ of a sphere of same volume [20], and it is related to the energy cost of making a bubble

$$I_Q = \frac{36\pi V^2}{S^3} = \left(\frac{S_0}{S}\right)^3. \tag{4}$$

For a sphere, the area is minimum and $I_Q = 1$. For a polyhedron, $I_Q$ is always less than 1 and as this value decreases the shape departs from a sphere; moreover, larger the $I_Q$, the more stable the bubble. For the ideal Kelvin cell $I_Q = 0.757$ and the average $I_Q$ of the Weaire and Phelan structure is $\langle I_Q \rangle = 0.764$. When calculated on all the 52 internal bubbles of young foam 2 and foam 3, $\langle I_Q \rangle = 0.694$ (standard deviation $= 0.034$); it is significantly lower than the value of any ideal structures. We have only plotted the $I_Q$ values for foams 2 and 3 for which all the bubbles, either entire or boundary, have been reconstructed as a function of the number of faces (Fig. 8) and of the pentagon percentage (Fig. 9) of the bubble. Weaire and Phelan still hold the championship of the bubble minimum surface area since no bubble has an $I_Q$ as high as the average value of their structure. However, one bubble in foam 3 has its $I_Q$ larger than the Kelvin tetrakaidecahedron ($I_Q = 0.757$); it is a bubble with 13 faces in the (3 6 4) combination (the more frequent one) for which $I_Q = 0.7603$. Another one with a (1 10 4) combination has a slightly lower $I_Q (= 0.7564)$ than the Kelvin one. However, other (3 6 4) bubbles have smaller $I_Q$. Actually, for the present foams, there is no obvious general relationship between the isoperimetric quotient of an individual bubble and its face combination (Table II), face number (Fig. 8), or percentage of pentagons (Fig. 9). The morphology of a bubble depends on the combination of its faces, on its metrics, and on collective effects with other ones through the fulfillment of the Plateau laws. Individually, the cells have no reason to have a minimum surface energy unless the foam is periodical like a Kelvin foam. In a Kelvin foam, collective effects are accounted for only in a trivial manner.

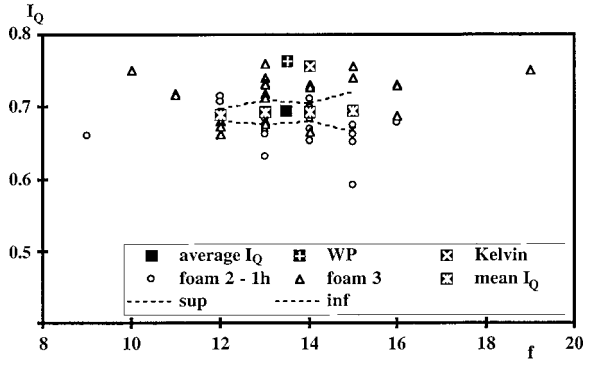


FIG. 8. Isoperimetric quotient versus the face number of the internal bubbles in young foams 2 and 3. $I_Q$'s for the Kelvin and Weaire and Phelan structures are reported. The solid line denotes the mean values and the dotted lines correspond to the mean value $\pm \Delta V$ (see Table II).

### D. Influence of the foam border

Matzke defined as internal bubbles those that are separated from the foam borders by at least three other bubbles and not by one bubble as used here [9]. During collapse, the influence of the film ruptures that were located at the foam surface did not extend to further layers. Average values of the topological elements of the internal bubbles did not vary significantly: $\langle f \rangle_{\text{int}} = 13.5 \pm 0.2$, $R_{\text{int}} = -0.23 \pm 0.005$ at $t \leqslant 9$ h and $t = 24$ h and 27 h. The tendency is the same at $t = 30$ h when only one bubble layer remains, but one should be cautious because the statistics become very poor. On the contrary, $R_{\text{ext}}$ drops to zero during foam aging. Since all the averaged topological properties of the internal bubbles (according to our definition) are stable one can state that a single bubble layer is enough to forget the singularity generated by the foam boundaries.

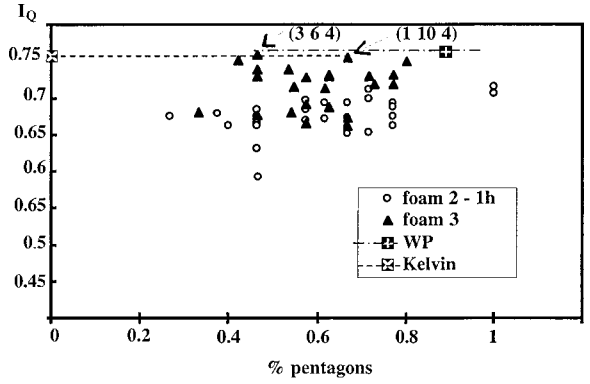


FIG. 9. Isoperimetric quotient versus the percentage of pentagons of the internal bubbles in young foams 2 and 3.

## V. CONCLUSION

The structure and the topology of young and ageing 3D foams with rigid films were investigated by optical tomography associated with a numerical reconstruction algorithm. We have confirmed the statistical data of Matzke on the mean numbers of faces and edges, and the present list of face combinations is essentially the same as the one found by Matzke. It seems obvious that some more original combinations could be found, however, with a low probability.

The original results on slightly polydisperse foams are the following. We have demonstrated that the disordered structure of the foam can be quantified by introducing a correlation coefficient between pairs of adjacent faces. It was found that the adjacent faces of internal bubbles are statistically slightly anticorrelated, the correlation coefficient being close to $-0.24$. We could not find any relationship between the isoperimetric quotient and the face combination in the bubbles, which means that the condition of mechanical equilibrium of the vertices is a much stronger requirement for the topology of the foams than the single minimization of the surface energy. We have assigned the absence of ideal structures in the real foam by their inadequate number of pentagonal faces: in the Kelvin cell, there are no pentagonal faces, and they are much more numerous in the Weaire and Phelan cluster than in a typical real foam. Eventually, one single bubble layer is sufficient to absorb the singularity created by the foam physical boundaries.

## ACKNOWLEDGMENT

Financial support from the Centre National des Etudes Spatiales is gratefully acknowledged.

[1] L. Oger, A. Gervois, J. P. Troadec, and N. Rivier, Philos. Mag. B **74**, 177 (1996).
[2] A. M. Kraynik, M. K. Neilsen, D. A. Reinelt, and W. E. Warren, in *Foams and Emulsions*, Vol. 354 of *NATO Advanced Studies Institute, Series E: Applied Sciences*, edited by J. F. Sadoc and N. Rivier (Kluwer, Dordrecht, 1999), p. 259.
[3] D. Weaire and S. Hutzler, *The Physics of Foams* (Cambridge University Press, London, 2000).
[4] D. Weaire and N. Rivier, Contemp. Phys. **25**, 59 (1984).
[5] W. Thomson, *Mathematical and Physical Papers* (Cambridge University Press, London, 1991), Vol. V, p. 297.
[6] R. W. Williams, Science **161**, 276 (1968).
[7] D. Weaire and R. Phelan, Philos. Mag. Lett. **70**, 345 (1994).
[8] D. Weaire, Recherche **26**, 246 (1995).
[9] E. Matzke, Am. J. Bot. **33**, 58 (1946).
[10] H. W. Schwarz, Rec. Trav. Chim. Pays-Bas. **84**, 771 (1965).
[11] C. Monnereau and M. Vignes-Adler, in *Foams and Emulsions* (Ref. [2]), Vol. 354.
[12] C. Monnereau and M. Vignes-Adler, J. Colloid Interface Sci. **202**, 45 (1998).
[13] C. Monnereau and M. Vignes-Adler, Phys. Rev. Lett. **80**, 5228 (1998).
[14] P. M. Kruglyakov, D. R. Exerowa, and K. I. Khristov, Langmuir **7**, 1846 (1991).
[15] K. J. Mysels, K. Shinoda, and S. Frankel, *Soap Films* (Pergamon, New York, 1957).
[16] C. Monnereau, M. Vignes-Adler, and N. Pittet, Philos. Mag. B **79**, 1213 (1999).
[17] K. Brakke, Exp. Math. **1**, 141 (1992).
[18] C. Monnereau, doctoral dissertation, University of Marne-la-Vallée, Champs-sur-Marne, France, 1998.
[19] A. G. Brown, W. C. Thuman, and J. W. McBain, J. Colloid Sci. **8**, 491 (1953).
[20] H. S. M. Coxeter, Ill. J. Math. **2**, 746 (1958).
[21] T. Aste, D. Boosé, and N. Rivier, Phys. Rev. E **53**, 6181 (1996).
[22] R. Phelan, D. Weaire, and K. Brakke, Exp. Math. **4**, 181 (1995).
[23] S. Ross and H. F. Priest, Colloids Surface **21**, 179 (1986).
[24] N. Pittet, N. Rivier, and D. Weaire, Forma **10**, 65 (1995).
[25] G. B. Han, A. Dussaud, A. Neimark, B. Prunet-Foch, and M. Vignes-Adler, J. Non-Equilib. Thermodyn. **25**, 325 (2000).
[26] J-F. Sadoc and R. Mosseri, *Aperiodicity and Order 3, Extended Icosahedral Structures* (Academic, New York, 1989).